A Partitioning Technique for a Waveform Relaxation Method Using Eigenvectors in the Transient Stability Analysis of Power Systems

Takao Tsuji, *Member, IEEE*, Frédéric Magoulès, *Member, IEEE*, Kenko Uchida, *Member, IEEE*, and Tsutomu Oyama, *Member, IEEE*

***Abstract*—It is of paramount importance that power system operators be able to assess transient stability in order to realize a reliable and stable power supply. Transient stability analysis can be formulated as a large-scale system of differential and algebraic equations (DAE). However, as power systems are becoming larger and more complex, it is becoming difficult to solve DAE in a practical amount of time for system operations. Parallel computing based on the waveform relaxation method is an effective solution to achieve faster calculations for transient stability analysis. To enhance the performance of the waveform relaxation method, a proper partitioning of the original problem is essential. Although various partitioning approaches have been used, those approaches might not be effective when analyzing a weakly damped low-frequency oscillation. In particular, in the Japanese 60-Hz power system, this oscillation becomes an important problem. To resolve this issue, in this paper we have developed a new partitioning method that is better suited to analyzing a weakly damped low-frequency oscillation based on eigenvalue analysis. Specifically, effective partitioning can be automatically determined by the proposed index, which can evaluate the validity of the partitioning. The proposed method was tested using the Japanese standards of the IEEJ WEST10 system model and the WEST30 system model.**

***Index Terms*—Eigenvalue analysis, parallel computing, power systems, transient stability, waveform relaxation method.**

I. Introduction

In order to secure a reliable and stable power supply, the N − 1 criterion is widely used as a reliability index for power system operations. A requirement of this criterion is that no outage should occur as the result of a single fault in a power system under thermal, voltage stability, frequency, and synchronous stability constraints. This means that system operators need to perform very heavy computing loads to check the above constraints under all credible faults. In particular, synchronous stability against a large disturbance, which is defined as transient stability analysis, is recognized as being very time consuming. A transient stability analysis can be formulated as differential and algebraic equations (DAE). As power systems are very large and complex, it is difficult to solve DAE in a practical amount of time to maintain stable system operation. Therefore, various parallel computing technologies have been studied to achieve faster calculations for transient stability analysis.

The application of the domain decomposition method to transient stability analysis has been studied as a parallel computing technique by Magoulès *et al.* In [1]–[3], an original problem is split into multiple subproblems in space, and each subproblem is assigned to a different processor to be solved in parallel. Although one subproblem cannot be solved independently from other subproblems because they interact with each other, the waveform relaxation method [4]–[9] enables the problems to be solved in parallel iteratively. In particular, in these references, initialization and preconditioning techniques are proposed to improve convergence. In addition, as shown in [10]–[12], the global problem is divided not only in space but also in the time domain by using the parareal method. It has been shown that the combination of system partitioning in both the space and the time domain works well for the transient stability analysis of power systems [11], [12].

In the waveform relaxation method, calculation time is strongly related to the validity of the system partitioning pattern in space. In addition, the desired partitioning pattern might change depending on the characteristic of the problem. Therefore, an automatic partitioning method is extraordinarily important, and thus many partitioning methods have been proposed for application in the waveform relaxation method. METIS algorithm [13], [14], which focuses on the topology of a network, is often applied to problems in power system analysis. However, in transient stability analysis based on variable-stepsize integration, the required size of the timesteps is determined by the steepest changing variable. If the system is divided considering the coherency of generators, a longer stepsize is available in subsystems where the maximum change rate is small [15], [16]. Therefore, a partitioning technique based on the coherency of generators is expected to provide an effective approach to reducing computing loads. Hence, for example, in [17] and [18], the coherency of generators is determined by using the proposed evaluation index, which

Manuscript received November 02, 2013; revised February 23, 2014; accepted September 23, 2014. Date of publication December 08, 2014; date of current version August 03, 2015. This work was supported by the Japan Science and Technology Agency (JST/CREST). Paper no. TPWRS-01400-2013.

T. Tsuji and T. Oyama are with the Faculty of Engineering, Yokohama National University, Hodogaya, Yokohama 240-8501, Japan (e-mail: t-tsuji@ynu.ac.jp).

F. Magoulès is with Ecole Centrale Paris, Paris, France.

K. Uchida is with Waseda University, Tokyo, Japan.

Color versions of one or more of the figures in this paper are available online at http://ieeexplore.ieee.org.

Digital Object Identifier 10.1109/TPWRS.2014.2362724

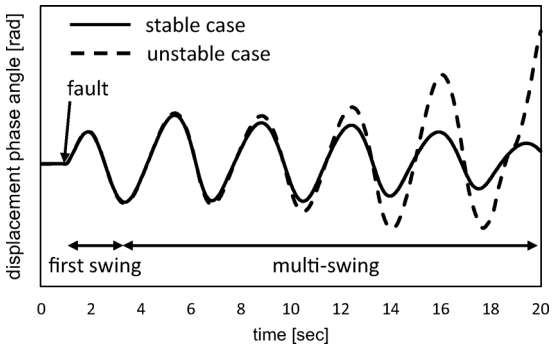

Fig. 1. First swing and multi-swing stability.

focuses on the displacement phase angle between generators shortly after the occurrence of a fault or the electrical distance from the fault point. In recent studies, independent component analysis and sensitivity analysis have been implemented to determine coherency [19]–[21]. In addition, the usage of a phasor measurement unit has also been studied [22].

Transient stability can be divided into two categories: first swing stability and multi-swing stability. The former is used to analyze the behavior of the system only at first power swing, while the latter is related to multiple power swings as shown in Fig. 1. Many partitioning methods for transient stability analysis as stated above focus, in the main, on first swing stability because this is more important when a power system is based on a mesh or loop configuration. However, multi-swing stability analysis also is important for some power systems, especially if the power system is based on a radial configuration. In practice, in the Japanese 60-Hz power system, a weakly damped low-frequency oscillation is generated by a fault, and this might trigger the multi-swing instability phenomenon. Fig. 1 shows two examples of this: a stable case and an unstable case. Although the step-out phenomenon does not occur in either of the cases at first swing, the oscillation barely converges after the second swing, and then step-out occurs in the unstable case. Thus, system operators have to analyze not only first swing but also multi-swing phenomenon, and it takes a long time to properly assess the stability. The oscillation of the excitation voltage controlled by an automatic voltage regulator (AVR) is related to this oscillation. However, with respect to this multi-swing stability analysis, the partitioning methods proposed in earlier papers might not be effective because their main aim is to analyze first swing stability, the characteristics of which are different from those of multi-swing stability.

It is known that the characteristics of a power swing can be predicted by eigenvalue analysis around the stable equilibrium point. Although the behavior of generators does not coincide with the eigenvalues completely under a large disturbance in transient stability analysis, there is a possibility that the coherency of all the variables can be explained roughly even when there is significant nonlinearity. Hence, in this paper, we developed a new partitioning method that is better suited to analyzing a weakly damped low-frequency oscillation based on eigenvalue analysis. Specifically, an effective partitioning can be determined by a proposed new index that can evaluate the validity of the partitioning by using the eigenvector.

The rest of this paper is organized as follows: In Section II, we outline transient stability analysis and its characteristics in the Japanese standard IEEJ WEST10 system model. In Section III, we describe the basis of the waveform relaxation method and also propose a new partitioning method that is better suited to analyzing weakly damped low-frequency oscillation. The effectiveness of the proposed method is tested in Section IV by using the WEST10 and the WEST30 system models. Finally, we present our conclusions in Section V.

II. Transient Stability in the Japanese 60-Hz Power System

A. Transient Stability Analysis

The behavior of synchronous generators and their controllers in power systems can be represented by differential equations, while the network calculation, including the stator side of generators, is represented by algebraic equations. Therefore, transient stability analysis can be formulated as DAE as follows:

$$\begin{cases} y' &= f(y,z,t),\ t \in [0,T] \\ 0 &= g(y,z,t) \end{cases} \tag{1}$$

where

f, g	functions of differential and algebraic equations;
y	differential variables;
z	algebraic variables;
t, T	elapsed time and total simulation time.

The specific equations used in DAE are shown in Appendix A. Usually, an iterative calculation is needed to solve an algebraic equation because the function g is nonlinear. Here, the voltage characteristics of active and reactive loads, which are strongly related to nonlinearity, are often modeled as constant current and constant impedance models, respectively. However, these models are based on statistical measurement data that focus on the steady states, and an accurate voltage characteristic in the transient state has not been clarified. In addition, transient stability tends to worsen when the voltage characteristic is treated as a constant impedance model, as compared to other models. As the power system model includes various uncertainties such as load change, it is important to err on the side of caution when assessing stability in order to ensure sufficiency. Hence, we make an assumption that the voltage characteristic of loads is represented by a constant impedance model in this paper. Under this assumption, the network model can be reduced and represented by simple linear equations given by a dense matrix. Therefore, the order of the computing load for solving this algebraic equation can be represented by the square of the matrix size, which is equal to the number of generators.

In order to solve DAE, the implicit Runge-Kutta method is used in this paper because it is suitable for solving stiff equations with adaptive stepsizes. Without using parallel computing, the problem is solved in chronological order, which is referred to as the sequential method in this paper.

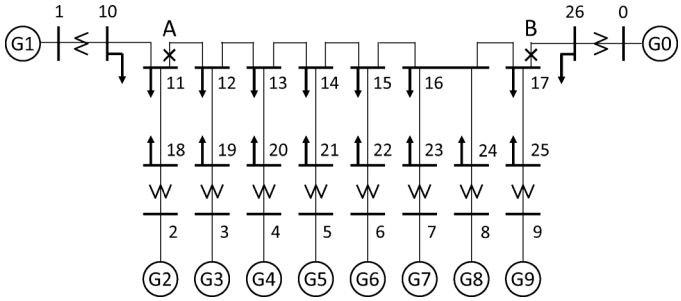

Fig. 2. IEEJ WEST10 system model (Japanese 60-Hz system model) [25].

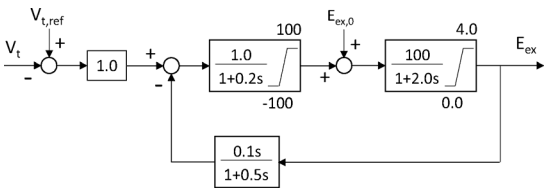

Fig. 3. Automatic voltage regulator. [25].

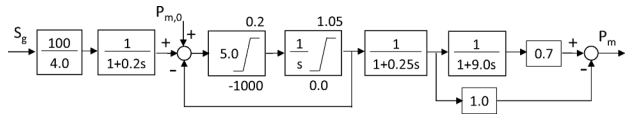

Fig. 4. Speed governor. [25].

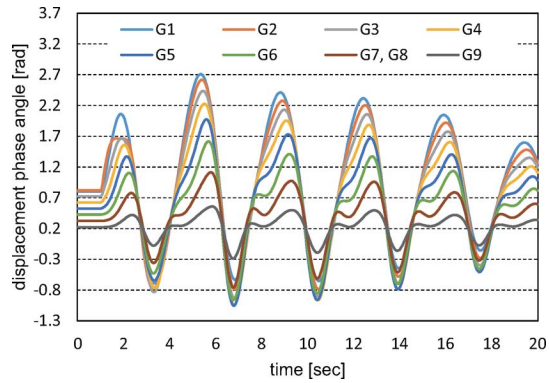

Fig. 5. Phase angle difference in case 1.

B. Weakly Damped Low-Frequency Oscillation in WEST10

Two power systems are used in Japan, a 50-Hz system in the east and a 60-Hz system in the west. The 60-Hz system has a longitudinal structure because western Japan is wider in the east-west direction. It is known that a weakly damped low-frequency oscillation occurs in this system, and that a simulation needs to be performed for longer to analyze this. As this tendency can be observed especially when the operating point is close to the stability boundary, increasing the speed of the analysis of this oscillation is of prime importance in determining the available transfer capability.

Against this background, the basic characteristics of transient stability in the Japanese 60-Hz power system is described in this section. It is known that we can simulate the above phenomenon in the Japanese 60-Hz power systems in the IEEJ WEST10 and WEST30 system models [23]–[25]. Both models are reduced models of the 60-Hz power system, and the scale of the WEST30 model is larger than that of the WEST10 model. Although utilization of a large-scale model better shows the effectiveness of the proposed method, it is not so easy to obtain a deep understanding of the phenomenon using a large-scale model. Therefore, the WEST10 system model is mainly used in this section to analyze the basic behavior of the Japanese 60-Hz power system. In the simulations described in Section IV, both the WEST10 and the WEST30 models are used in order to show the effectiveness of the proposed method.

Figs. 2–4 show the network structure and controllers equipped with generators (automatic voltage regulator: AVR, and speed governor: GOV). There are 10 generators and 27 nodes. Each generator, including the AVR and GOV, is modeled as differential equations with a total of 13 orders. As all the nodes other than the generator bus are reduced, the number of variables in an algebraic equation is 40 (four variables per generator bus: voltage and current in the direct and quadrature axes).

To analyze the relationship between the fault conditions and the characteristics of power swing, the following two fault cases were examined:

Case 1: fault point A (fault clearing time 80 msec)

Case 2: fault point B (fault clearing time 140 msec)

Because the transient stability is more severe in the case of a fault at the west end, the fault clearing time is adjusted to be smaller in case 1.

Fig. 5 shows the displacement phase angle in case 1, where the phase angle of G0 is treated as a reference. Because the fault point is near the west end of the system, G1 and G2 fluctuate significantly compared to the other generators shortly after the fault occurrence. As the system condition is close to the stability boundary, the magnitude of the oscillation does not decrease quickly.

Fig. 6 shows the phase angle of all the generators in case 1. Not only the displacement phase angle, but also the phase angle is important when discussing the calculation time because the available stepsize in the integration by the implicit Runge-Kutta method is determined by the maximum change rate among all variables. We can see from this figure that all the generators are oscillated by this fault. In particular, the oscillation of generators on the east side, such as G0 and G9, is very large. Hence, in the WEST10 system model, we can estimate that the conventional partitioning approaches, in which the size of subsystems are adjusted to be larger at a distant area from the fault point, do not work effectively.

Fig. 7 shows the fluctuation of excitation voltage controlled by the AVR. The timing of the fluctuation differs from that in the phase angle. Although many partitioning techniques are based on coherency only considering the phase angle, we can see from this figure that a consideration of other variables is also important to recognize the maximum change rate.

Fig. 8 shows the displacement phase angle in case 2. Although the large fluctuations are caused by the fault in the

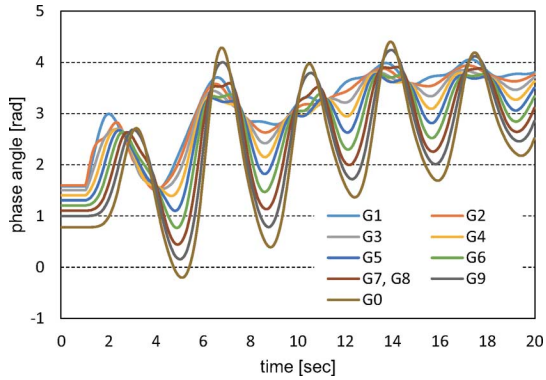

Fig. 6. Phase angle in case 1.

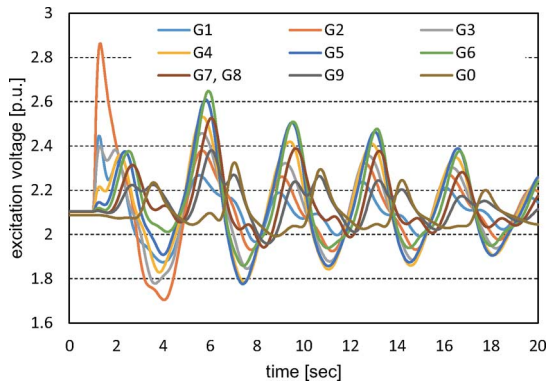

Fig. 7. Excitation voltage in case 1.

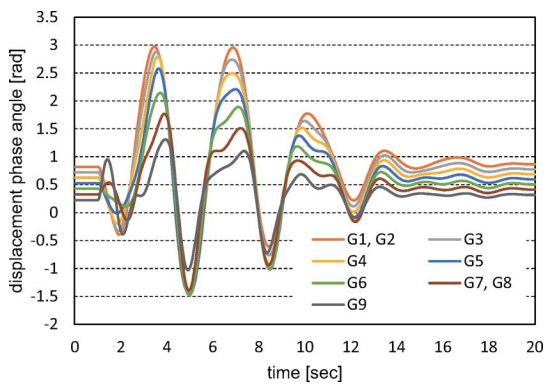

Fig. 8. Phase angle difference in case 2.

eastern generators just after the disturbance, the same coherency as that in case 1 can be seen after the second oscillation. This tell us that these characteristics are inherent to the power system characteristics. Specifically, there is a possibility that eigenvalue analysis around the stable equilibrium point is effective in predicting behavior in the time domain of multi-swing stability, regardless of the fault point.

C. Eigenvalue Analysis

The placement of the eigenvalues in this system is shown in Fig. 9. Generally, the conjugate eigenvalue whose damping is weakest has a great impact on synchronous stability. In this case, there is one pair of conjugate eigenvalues whose damping

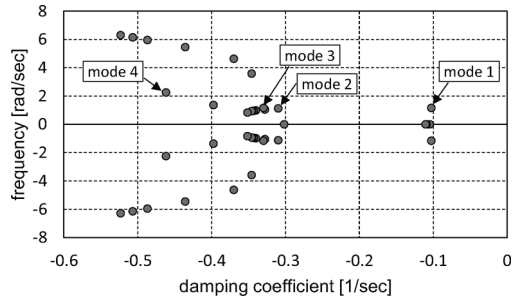

Fig. 9. Eigenvalues of WEST10 system model.

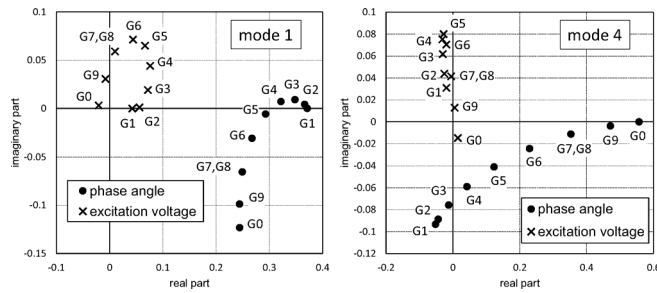

Fig. 10. Eigenvectors related to phase angle and excitation voltage.

is weakest (mode 1) around (−0.1 [1/sec], 1.1 [rad/sec]). In addition, it is known that an autoparametric resonance[26] occurs between some modes whose frequency are equal to the integral multiple each other. In the WEST10 system model, frequency of modes 2, 3 and 4 are equal to the integral multiple of that of mode 1. Therefore, these modes are oscillated with mode 1, and weakly damped low-frequency oscillation is caused by this autoparametric resonance as shown in Fig. 5. As described above, the weakly damped low-frequency oscillation caused by the interaction of multiple modes is defined as the dominant mode in this paper.

The eigenvectors corresponding to mode 1 and 4 are shown in Fig. 10. In practice, a single right eigenvector relates its associate oscillation mode to all the state variables. However, only the state variables related to phase angle and excitation voltage are shown in this figure because the magnitude of factors related to these variables is much larger than that of the other factors. Based on this analysis, we can estimate the behavior of the system in the linear region around the equilibrium point. Fig. 11 shows the one cycle of the estimated oscillations related to the phase angle and the excitation voltage. Here, they are derived by composition of the above four modes supposing that amplitudes and phase angle of their modes are the same. Compared to Figs. 6 and 7, we can see that tendency of the coherency can be well predicted by eigenvalue analysis, although their behavior does not coincide perfectly due to the impact of the nonlinear characteristics. By utilizing this fact, a new partitioning approach based on the eigenvalue analysis is discussed in Section III.

Finally, the robustness of the eigenvalue analysis is discussed below. Both eigenvalues and eigenvectors can change depending on the operating point, such as load change or network reconfiguration caused by the actions of protective relays. Fig. 12 shows the estimated dominant swing mode

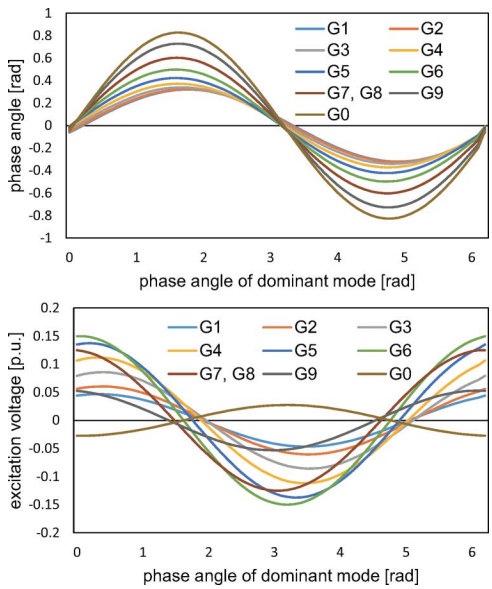

Fig. 11. Linear prediction by using eigenvectors (original system).

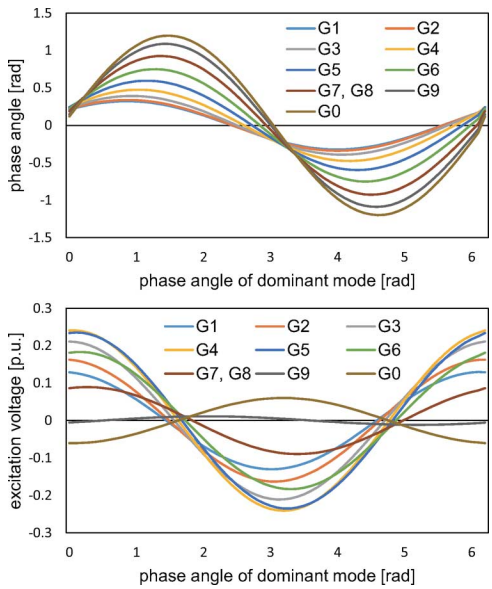

Fig. 12. Linear prediction by using eigenvectors (load change case).

related to phase angle and excitation voltage supposing that all the loads and generation output are reduced by 10%. Here, the dominant mode is composed by some modes which are corresponding to from mode 1 to mode 4 in the original system. Actually, the maximum change rate of the generating output in conventional thermal generating plants is around 10%/10 min. Considering that the change rate is smaller in the case of some other generating plants such as nuclear power, this setting can be regarded as a kind of worst case in which the system load changes rapidly in 30 min or 1 h. From Figs. 11 and 12, we can see the tendency of the coherency do not change largely, although the order of the coherency becomes different in some generators regarding excitation voltage. Here, it should be also noted that the amplitude of the oscillation is not important.

From a viewpoint of recent penetration of distributed generators such as photovoltaic generations and wind turbines, the system state might change faster than above assumption due to their uncertain and rapid fluctuation. In particular, if systems include many wind firms and their output change dramatically, for example, due to the cut-off operation of wind turbines, its impact would be given to the eivenvectors. However, in this study, it is supposed that the proposed method is mainly applied to Japanese power system, and the main target of the renewable energy integration is photovoltaic generations in Japan. Hence, the above situation is not considered in this paper supposing that the smoothing effect works effectively by the uniformed distribution of photovoltaic generations.

Next, the impact by the system reconfiguration was also tested supposing the transmission line between node 11 and node 12 was decreased by half. As many transmission lines are reduced and represented by a single line in the WEST10 system model, this assumption should be sufficiently large. However, even under such a large disturbance, the difference in the dominant mode was limited to the same extent though the results are omitted here.

As above, in the case of the Japanese 60-Hz power system, we can see that there is a strong robustness in the eigenvalue analysis. Although it is better to recalculate the eigenvector according to the change of the operating point, the same eigenvector would be also available during several hours when the recalculation is not in time.

III. Partitioning Technique for Waveform Relaxation Method

In the waveform relaxation method, the original system is split into multiple subsystems, and each problem is independently solved by the sequential method in parallel by different processors. After calculations at all subsystems have finished, the waveforms are exchanged between neighboring subsystems, and a converged solution is obtained by repeatedly applying this procedure. Therefore, the required calculation time in each iteration depends upon the maximum calculation time in all the subsystems as the Gauss-Jacobi algorithm is applied in this paper (see Appendix B for details). In other words, a balanced computing load on all processors is important to achieve an increase in speed, and the load balance strongly depends on the partitioning. Hence, the purpose of the partitioning method is to improve the load balance between all subsystems to maximize the advantage of the adaptive stepsize control in the implicit Runge-Kutta method.

The setting for the interface condition is shown in Fig. 13. This is an example in which the global system is divided into two subsystems at branch 14–15. As shown in this figure, the overlap concept is applied in this paper. Namely, the waveforms, which are the voltage fluctuation at nodes 14 and 15, are calculated independently in subsystems 1 and 2, respectively, and they are updated at the end of each iteration (in addition, the waveforms at nodes 14 and 15 are used in subsystems 2 and 1, respectively). For image-building, virtual generators are introduced to the nodes at which the waveforms are used. Apart from the fact that synchronous reactances do not exist, these virtual

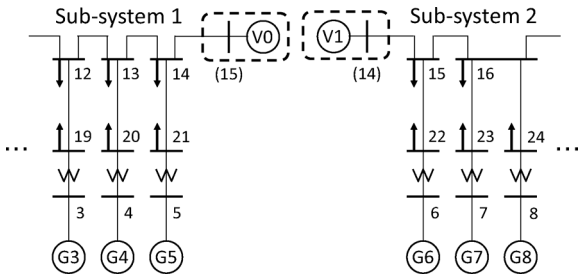

Fig. 13. Example of interface condition.

generators are treated the same way as other synchronous generators in algebraic equations.

As denoted in Section II, the coherency of variables tends to be determined mainly by the dominant swing mode represented by its corresponding eigenvector several seconds after the fault clearing time. Hence, the computing load on each processor can be estimated in advance supposing that the power swing caused by a fault is similar to the fluctuation of the dominant swing mode. The behavior of the dominant swing mode is formulated as

$$x_{i,j} = |r^*_{i,j}| \sin(\theta + \delta_{i,j}) \tag{2}$$

where $x_{i,j}$ is the estimated state variable at generator i, variable j, and $r^*_{i,j}, \delta_{i,j}$ is the magnitude and phase angle of the dominant eigenvector at generator i, variable j.

Of course, the behavior of the power swing is more complex because the transient phenomenon includes various swing modes and they interact with each other due to the nonlinearity. However, it can be expected that the above idea will work well in a case where a major swing mode can be detected as most of the other modes decrease rapidly and the substantial characteristic is represented by the dominant mode.

Let us consider the following assumptions:

- The dominant mode continues to oscillate without decreasing its amplitude. In other words, the damping rate is not considered.
- The required number of calculation steps is proportional to the maximum change rate in all the variables included in the same subsystem. The validity of this assumption is discussed using a simulation in Section IV
- In the implicit Runge-Kutta algorithm, it is needed to solve linear simultaneous equation. Generally, the amount of calculation for this process can be represented as cubic function. Therefore, the computing load at each timestep is proportional to the cube of the number of generators included in the same subsystem.
- The computation time in each time window is determined by the maximum calculation time in all the subsystems because the Gauss-Jacobi algorithm is applied.

Under the above assumptions, the computing load in each subsystem is proportional to the product of the estimated number of calculation steps based on the maximum change rate and the cube of the number of generators including in the subsystem. The maximum change rate is derived by differentiating (2) with respect to θ supposing that the dominant swing mode fluctuates at a constant speed. Hence, the degree of the computing load can be evaluated by the following evaluation index, EI:

$$EI = \max_{s \in SD} \int_0^{2\pi} \left\{ a \max_{i \in G_s, j \in V_G} |r^*_{i,j}| \cos(\theta + \delta_{i,j}) + b \right\} g_s^3 d\theta \tag{3}$$

where

SD	set of subsystems;
G_s	set of generators in subsystem s;
V_G	set of variables in each generator;
g_s	number of generators in subsystem s;
a, b	slope and intercept of the approximate line in the relationship between required number of steps and maximum change rate.

Based on these results, we can estimate optimal partitioning using the following procedures:

A. Connection Diagram

The method proposed in this paper should be mainly applied to power systems that are based on a radial configuration because the multi-swing stability is more important in those power systems. To clarify the positional relationship between generators in radial power systems, a connection diagram in which all the generators are numbered in series is effective. For example, although the WEST30 system model includes a loop configuration in part, the positional relationship between generators can be treated as shown in Fig. 14. Incidentally, the connection diagram for the WEST10 system model is omitted as it is obvious. The italic numbers next to the generator numbers represent the partitioning points. If we divide the system into n subsystems, we have to specify at least $n-1$ partitioning points. Although an initial partitioning pattern can be determined arbitrarily, it would be reasonable to specify the partitioning points in order that the number of generators included in each subsystem be almost the same because the load balance between subsystems is important to enhancing calculation speed. In this example, the system is divided into 6 subsystems by specifying five partitioning points, 3, 6, 9, 12, and 19. For a better understanding of the connection diagram, some denotations are defined below. A partitioning point that is on the border of subsystems i and j is denoted as $p_{i,j}$. A partitioning pattern can be represented as a set of partitioning points, for example in this case, $P = \{p_{1,2}, p_{2,3}, p_{3,4}, p_{4,5}, p_{4,6}\} = \{3, 6, 9, 12, 19\}$. In addition, a set of adjacent partitioning points around $p_{i,j}$, $A_{i,j} = \{a_{i,j,k}\}$, $k = 0 \ldots m$, is defined. For example, the set of adjacent partitioning points of $p_{1,2}$ is represented as $A_{1,2} = \{2, 4\}$. These definitions are used in the flowchart described later.

B. Eigenvalue Analysis

The eigenvalues and eigenvectors are calculated in advance. However, this process should be carried out also for other purposes such as PSS design. Thus, it should be noted that an additional computing load is not needed during actual system operation. The dominant mode is composed by some corresponding eigenvectors, whose frequency are equal to the integral multiple of the conjugate eigenvalue with the largest damping rate. Here,

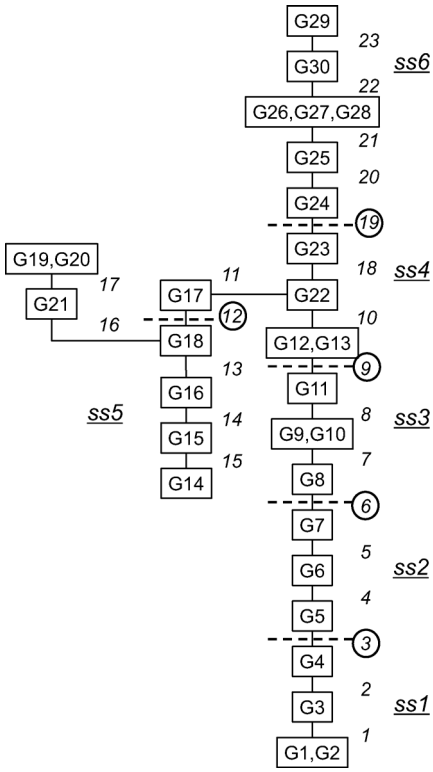

Fig. 14. Positional relationship in WEST30.

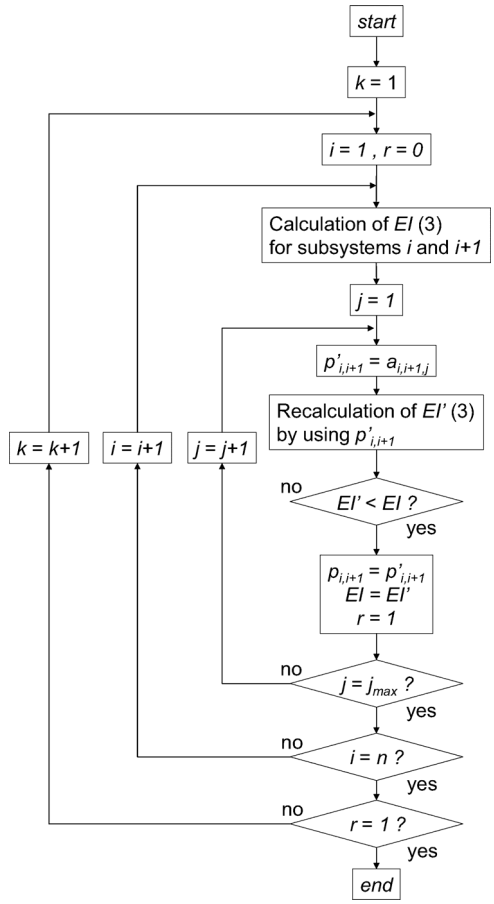

Fig. 15. Flowchart of the proposed method.

if needed, knowledge of the characteristics of the system could be considered to choose the corresponding eivenvectors.

C. Search Algorithm

To search for the optimal partitioning pattern, the following iterative procedure is introduced. First, the evaluation index is calculated for all the subsystems based on a specified initial partitioning pattern. Next, the evaluation index is recalculated by shifting each partitioning point in order to improve the evaluation index. Specifically, in the case of Fig. 14, partitioning point 3 is virtually shifted to 2 and 4, and the evaluation index is recalculated only within subsystems 1 and 2 for both cases. If either change improves the evaluation index, the partitioning point is shifted to that direction. The same procedure is applied to all the other partitioning points, and, if at least one change is executed, the same procedure is iterated again. If there is no change, the partitioning pattern becomes a converged solution that cannot be improved anymore. The flowchart of this search algorithm is shown in Fig. 15.

IV. Simulation Results

A. System Model and Specifications of Waveform Relaxation Method

We performed simulations to show the effectiveness of the proposed method using both the WEST10 and the WEST30 system models. Although simulations using other large models such as the European interconnected power system model are also important, we choose the Japanese power system model because the proposed method is effective mainly for systems based on a radial configuration.

The Gauss-Jacobi algorithm with an overlap in interface conditions is used. To enhance convergence, all the waveforms are specified before the first iteration by the initialization technique, and are modified at the end of each iteration by the preconditioning technique[1]–[3]. The entire time domain, 20 [sec], is divided into 50 time windows. The size of each time window is 0.4 [sec]. The maximum stepsize in the implicit Runge-Kutta method is 20 [msec]. Thus, at least 20 steps are required in each time window. The threshold value used to determine the convergence is set to 0.001 considering the accuracy of the calculation as denoted later. Finally, the number of available processors (CPUs) is 4 and 6, in the WEST10 model and the WEST30 model, respectively. If a large number of CPUs are available, we can assign multiple CPUs for the analysis of each subsystem, and the parallel computing technique should be used to speed up the matrix calculation. However, this kind of parallel computing is applicable independently from the proposed partitioning method. Hence, in this paper, we supposed that the original system is divided into the same number as the number of CPUs because we can show the effectiveness of parallel computing by focusing only on the partitioning technique. The communication time between subsystems is set to 50 [msec].

B. Relationship Between Change Rate and Required Number of Steps

In the previous section, we worked under the assumption that the required number of calculation steps is proportional to the

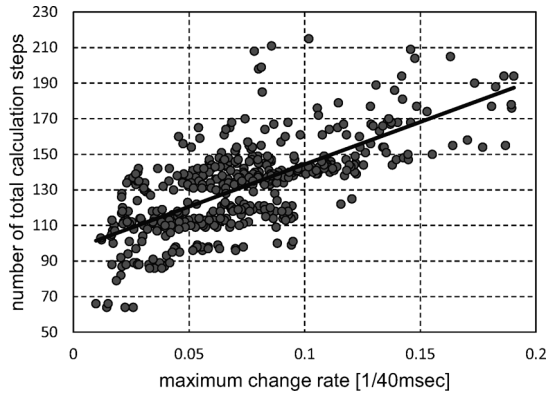

Fig. 16. Required number of steps and maximum change rate.

TABLE I
PARTITIONING PATTERNS (WEST10)

	generators included in each subsystem (node number of virtual generators)			
pattern 1	1,2,3	4,5	6,7,8	9,0
	(13)	(12),(15)	(14),(17)	(16)
pattern 2	1,2	3,4,5	6,7,8	9,0
	(12)	(11),(15)	(14),(17)	(16)
pattern 3	1,2,3	4,5,6	7,8	9,0
	(13)	(12),(16)	(15),(17)	(16)
pattern 4	1,2	3,4	5,6	7,8,9,0
	(12)	(11),(14)	(13),(16)	(15)
pattern 5	1,2,3,4	5,6	7,8	9,0
	(14)	(13),(16)	(15),(17)	(16)
pattern 6	1,2	3,4,5,6	7,8	9,0
	(12)	(11),(16)	(15),(17)	(16)

maximum change rate in all state variables. Before showing the simulation results obtained with the waveform relaxation method, the validity of this assumption is discussed in this subsection. Regarding case 1 as shown in Section II, Fig. 16 shows the scatter graph of the number of calculation steps and the maximum change rate. We can see from this figure that their relationship is almost linear, and we can specify the approximate straight line as shown in the figure, whose slope and intersect are 96.82 steps/40 msec and 475.6 steps, respectively.

C. Simulation Results in the WEST10 System Model

The proposed partitioning technique is applied to the Japanese WEST10 system model with two simulation cases, the details of which are shown in Section II. Because only 10 generators are included in this model, the number of candidates for the partitioning pattern is small. If there is a subsystem that includes only one generator, the load balance is not correct, obviously. Hence, by skipping such candidates, we applied the six partitioning patterns shown in Table I. The proposed evaluation index and calculation time in each simulation case are shown in Tables II and III. To analyze the effectiveness on first and multi-swing stability, the calculation times for tw=0–6 and tw=7–49 are listed separately. The figure within ( ) represents the ranking of the validity of the partitioning in each simulation case.

We can see from these tables that the proposed evaluation index works well because the ranking of the partitioning patterns can be predicted in the period of time for multi-swing

TABLE II
EI AND CALCULATION TIME IN CASE 1 (WEST10)

	EI	tw=0-6	tw=7-49
without WR	-	83.88 sec	586.43 sec
partitioning 1	1.19 (2)	18.64 sec (3)	127.25 sec (3)
partitioning 2	1.19 (2)	15.41 sec (1)	122.01 sec (2)
partitioning 3	1.00 (1)	18.44 sec (2)	121.66 sec (1)
partitioning 4	3.78 (6)	22.81 sec (4)	237.50 sec (6)
partitioning 5	1.80 (4)	36.34 sec (6)	193.03 sec (4)
partitioning 6	2.37 (5)	28.51 sec (5)	228.25 sec (5)

TABLE III
EI AND CALCULATION TIME IN CASE 2 (WEST10)

	EI	tw=0-6	tw=7-49
without WR	-	113.72 sec	511.5 sec
partitioning 1	1.19 (2)	18.74 sec (3)	96.03 sec (3)
partitioning 2	1.19 (2)	17.51 sec (2)	93.98 sec (2)
partitioning 3	1.00 (1)	16.21 sec (1)	93.73 sec (1)
partitioning 4	3.78 (6)	44.27 sec (6)	189.46 sec (6)
partitioning 5	1.80 (4)	25.24 sec (4)	149.14 sec (4)
partitioning 6	2.37 (5)	30.08 sec (5)	163.93 sec (5)

stability except the ranking 2 and 3. Here, although the partitioning pattern 2 is better than pattern 1, the proposed method can not predict this order properly. This is due to the fact that the estimated oscillation based on the eigenvalue analysis has a margin of error. Specifically, phase angle of generators near the west-end, such as G1 and G2, do not actually fluctuate in the multi-swing region as shown in Fig. 6. However, this behavior is not predicted by the eigenvalue analysis as shown in Fig. 11. Since it is estimated that their phase angle are also oscillated, the pattern 1, in which the subsystem 1 has three generators, was evaluated poorly than in reality.

Regarding the time domain corresponding to the first swing, the ranking estimated by the proposed method does not coincide with the actual simulation results. This is due to the influence of nonlinearity in the first power swing. As for the first swing, it is expected that the phase angle moves wider as the generator is closer to the fault point. Therefore, it should be noted that conventional methods, in which the partitioning pattern is decided based on behavior shortly after the fault or the electrical distance from the fault point, work more effectively for first swing stability analysis. By dividing the original system into subsystems, it is possible to reduce the stepsize in the implicit Runge-Kutta method in subsystems with a changing rate that is not large. Due to this effect, the speed increase in both cases was more than 4.0 with four CPUs.

Although the waveform relaxation method is effective in increasing speed, it is possible that the calculation accuracy decreases in the case of an insufficient threshold value for a convergence check. Fig. 17 shows the error between the waveform relaxation method and the sequential method. Due to the accumulation of small errors, the calculation error becomes larger with time. However, we can see from this figure that it is not so large and it is assumed that the magnitude of the error is permissible for actual system operation. The error can be reduced by decreasing the threshold value for the convergence check. Next, Fig. 18 shows the calculation time in each time window regarding the partitioning pattern 3 and pattern 2, the

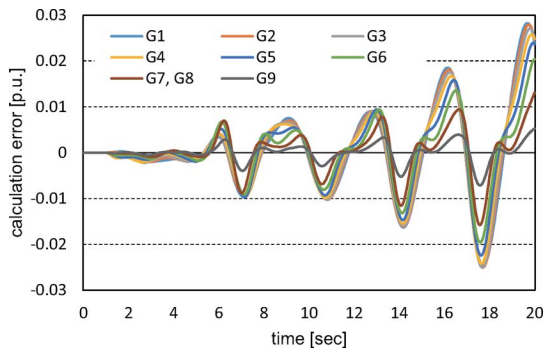

Fig. 17. Calculation error in case 1.

performances of which were the best and second best, respectively. Although the size of each time window was the same, the required calculation times were different because the required number of timesteps changed depending on the change rate of the variables. In partitioning pattern 3, the calculation time of CPU1 was relatively longer during the initial period of time because subsystem 1 included three generators in pattern 3, while it included two generators in pattern 2. However, the calculation time of CPU1 is not so important because it was sufficiently small after the first swing and the performance should be evaluated considering the dominant long period swing mode. Conversely, for CPU3, the calculation time was smaller in the case of pattern 3 because subsystem 3 included two generators in this pattern. As a result, total calculation time can be made smaller by improving the load balance between CPUs by choosing partitioning pattern 3 as opposed to pattern 2.

Fig. 19 shows the number of iterations in each time window in case 1 with partitioning pattern 3, whose performance was the best, and pattern 4. The partitioning idea with pattern 4 was similar to that of conventional approaches in which the coherency only in the initial period of time was considered because the size of the subsystem was adjusted to be larger at the side distant from the fault point. Specifically, the number of generators was two in all subsystems except for subsystem 4, which had four generators. Due to the work involved in the preconditioning and initialization methods, the number of iterations was limited to five in the case of pattern 3. However, the number of iterations was slightly smaller in the case of pattern 4 in the latter period of time. The fact shows that the load balancing technique leads to the additional interaction between processors. If this interaction has a high impact on the required number of iterations, there is a possibility that the speedup obtained by the load balancing would be decreased. Although this problem was not severe in the simulation cases in this paper, it must be treated carefully in applying the proposed method.

Finally, Fig. 20 shows a comparison of the cumulative calculation time at each time window between pattern 3 and pattern 4. The figure shows that the calculation time is shorter in the case of pattern 4 during the initial period of time, especially during the first and second swing before 4.0 [sec]. After that, however, the proposed partitioning approach was better because the load balance between CPUs over a long period of time was considered in the proposed method.

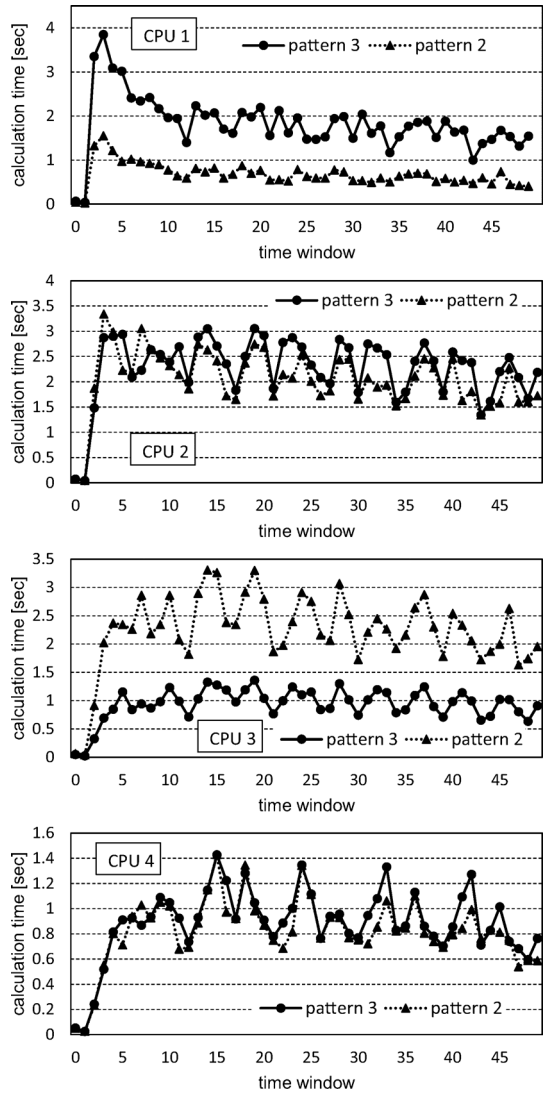

Fig. 18. Calculation time at each time window.

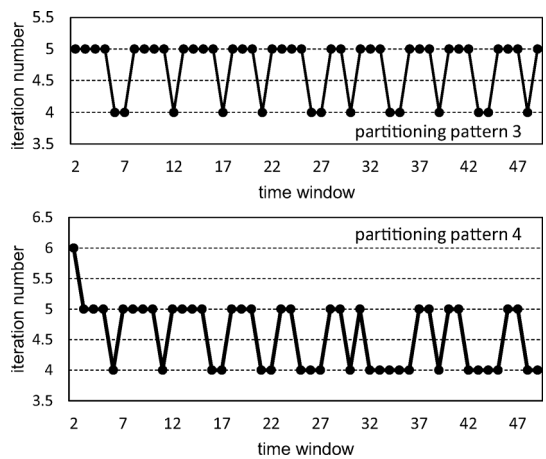

Fig. 19. Iteration number at each time window (case 1—pattern 3 and 4).

D. Simulation Results in WEST30 and EAST30 System Model

The transient stability analysis is performed on the WEST30 system model supposing that a three-phase short-circuit fault occurs near generator 4 and that the fault clearing time is 50

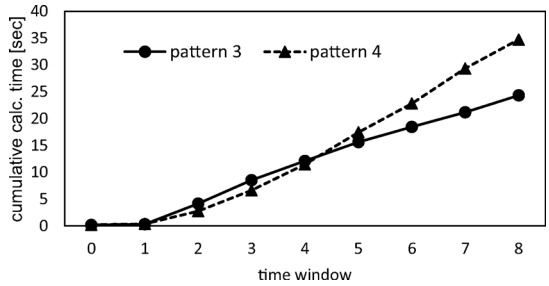

Fig. 20. Cumulative calculation time at each time window.

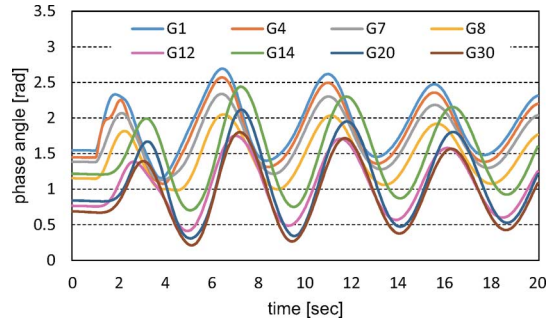

Fig. 21. Phase angle (WEST30).

msec. Here, parameters of all the generators are set to the same values for simplicity. Fig. 21 shows the phase angle for this model. As with the case in the WEST10 model, we can see a large disturbance throughout the systems. The proposed method was applied to the WEST30 system model. The initial partitioning pattern was set as $P = \{18, 19, 20, 21, 22\}$ in Fig. 14. The simulation result is shown in Table IV. Here, the optimal partitioning pattern obtained by the proposed method is $P = \{3, 7, 10, 12, 21\}$. The speed increase obtained by the proposed method was around 10-fold using 6 CPUs. As above, we can see that the proposed method is more effective in analyzing multi-swing stability by using a long period of time.

On the other hand, the simulation was also performed in the EAST30 system model [23]–[25] supposing that a three-phase short-circuit fault occurs near generator 1 and 4 (point B) [25] and that the fault clearing time is 150 msec. The EAST30 system model was the standard power system model of 50-Hz network in the eastern Japanese power system based on the meshed configuration. As with the WEST30, parameters of all the generators are set to the same values for simplicity.

Fig. 22 shows the phase angle change for this model. Compared to the simulation cases with WEST10 and WEST30 system models, the size of the oscillation is smaller after the third swing while the size of the first swing is larger.

We prepared two simulation cases whose partitioning patterns are shown in Table V. Pattern 1 was determined considering the coherency of the power swing around stable equilibrium point without using the search Algorithm in Section III because the search method was proposed for the systems based on radial configurations. However, in this case, almost all of the generators fluctuate as one coherent group as shown in Fig. 22. Therefore, the number of generators included in each subsystem is simply adjusted to be the same (7 or 8). Pattern 2 was based on the coherency right after the fault is cleared in order to increase calculation speed for first swing stability analysis. To this end, the number of generators in subsystem 4 is reduced while it is increased in subsystem 1 which is the farthest from the fault point.

Table VI shows the calculation time with both patterns. The calculation speed is faster in the case of pattern 1. However, the effectiveness of taking the long-term coherency into consideration is smaller in the EAST30 compared to the WEST30 because the damping rate is larger in this case. In addition, the calculation speed of pattern 1 is faster even during the first swing because the phase angle increases right after the fault even in subsystem 1. Hence, regarding not only the multi-swing stability but also the first swing stability, the calculation burden becomes larger at subsystem 1 in the case of pattern 2. From this simulation case, we can see that the weakly damped low-frequency oscillation becomes more important problem and the proposed method would be more effective in the power systems with radial configurations.

TABLE IV
EVALUATION INDEX AND CALCULATION TIME IN WEST30 MODEL

	tw=0-6	tw=7-49
without WR	312.1 sec	3096 sec
proposed method	32.8 sec	298.5 sec

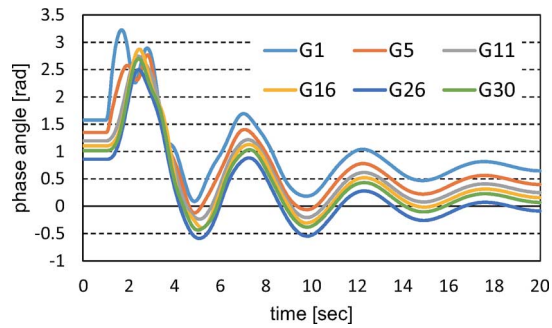

Fig. 22. Phase angle (EAST30).

TABLE V
PARTITIONING PATTERNS (EAST30)

	generators included in each subsystem	
	pattern 1	pattern 2
subsystem 1	24,25,26,27	20,21,24,25,26
	28,29,30	27,28,29,30
subsystem 2	8,9,10,11	7,8,9,10
	20,21,22,23	11,22,23
subsystem 3	12,13,14,15	12,13,14,15
	16,17,18,19	16,17,18,19
subsystem 4	1,2,3,4	1,2,3,4
	5,6,7	5,6

TABLE VI
CALCULATION TIME IN EAST30 MODEL

	tw=0-6	tw=7-49
pattern 1	151.5 sec	702.3 sec
pattern 2	188.3 sec	901.2 sec

V. Conclusion

Parallel computing technology is massively important in realizing the fast analysis of transient stability of very large and complex power systems. The waveform relaxation method is an important technique for this purpose, and an effective partitioning method is essential to maximizing performance. In this paper, a new partitioning technique, which is appropriate for a calculation over a relatively long period of time, was proposed considering application to the Japanese power system. The method is based on a eigenvalue analysis and its effectiveness was tested using the Japanese power system models. The following knowledge was obtained through the simulation:

- By applying the waveform relaxation method with the proposed partitioning method to the Japanese 60-Hz system model, the obtained speed increase is more than the number of CPUs because a longer size for the calculation step can be allowed.
- The coherency of the power swing is different depending on the fault point especially during the initial period of time. However, after several oscillations have finished, the same coherency as based on the eigenvector can be observed. Therefore, in the analysis of weakly damped low-frequency oscillation, it was shown that the proposed method worked effectively regardless of the fault point.

Areas of future work are as follows:

- The proposed method in this paper is applicable mainly for systems based on a radial configuration. We should improve our proposed method so that it can work for systems based on a mesh configuration or a loop configuration. In addition, there is a possibility that the search algorithm stops at the local solution. Therefore, it should be important to develop the global search algorithm.
- In this paper, the number of subsystems, which is the same as the number of CPUs, was given. However, the number of subsystems is also an important factor in determining the calculation performance of the waveform relaxation method. Therefore, the proposed method should be improved so that it can determine the optimal number of subsystems.
- It was shown that the conventional approach was better than the proposed method for analysis in a short period of time. Hence, the proposed approach should be developed so that there is automatic adjustment of the partitioning, which would enhance the calculation efficiency by changing the partitioning pattern from the conventional one to the proposed one at appropriate timing.
- The waveform relaxation method can be applied also in the time domain. Automatic partitioning should be done not only in space but also in time for maximum utilization of the CPUs.
- The voltage characteristic of loads is treated as a constant impedance in this paper. However, the proposed method needs to be able to treat other load models such as constant current and constant power.

Appendix A
Basic Equations for Transient Stability Analysis

Differential Equations [27]: The following differential equations are used in this paper to model the behavior of the synchronous generator:

$$\frac{d\delta}{dt} = \omega - \omega_0 \tag{4}$$

$$\frac{d\omega}{dt} = \frac{1}{M}\left[\frac{\omega_0}{\omega}\{P_m - P_e\} - D\{\omega - \omega_0\}\right] \tag{5}$$

$$\begin{aligned}\frac{de'_q}{dt} = \frac{1}{T'_{do}}\Bigg[&e_f + \frac{(L_d - L'_d)(L'_d - L''_d)}{(L'_d - L_l)^2}K_d e''_q \\ &- \left\{1 + \frac{(L_d - L'_d)(L'_d - L''_d)}{(L'_d - L_l)^2}\right\} e'_q \\ &- \omega\frac{(L_d - L'_d)(L''_d - L_l)}{(L'_d - L_l)} i_d\Bigg]\end{aligned} \tag{6}$$

$$\frac{de''_q}{dt} = -\frac{1}{T''_{do}K_d}\left\{K_d e''_q - e'_q + \omega(L'_d - L_l)i_d\right\} \tag{7}$$

$$\begin{aligned}\frac{de'_d}{dt} = -\frac{1}{T'_{qo}}\Bigg[&-\frac{(L_q - L'_q)(L'_q - L''_q)}{(L'_q - L_l)^2}K_q e''_d \\ &+ \left\{1 + \frac{(L_q - L'_q)(L'_q - L''_q)}{(L'_q - L_l)^2}\right\} e'_d \\ &- \omega\frac{(L_q - L'_q)(L''_q - L_l)}{L'_q - L_l} i_q\Bigg]\end{aligned} \tag{8}$$

$$\frac{de''_d}{dt} = -\frac{1}{T''_{qo}K_q}\left\{K_q e''_d - e'_d - \omega(L'_q - L_l)i_q\right\} \tag{9}$$

$$K_d = 1 + \frac{(L'_d - L_l)(L''_d - L_l)}{(L'_d - L''_d)(L_d - L_l)} \tag{10}$$

$$K_q = 1 + \frac{(L'_q - L_l)(L''_q - L_l)}{(L'_q - L''_q)(L_q - L_l)} \tag{11}$$

where

δ	phase angle difference;
ω, ω_0	rotor speed and its reference value;
M, D	inertia constant and damping coefficient;
P_m, P_e	mechanical input and electrical output;
e'_q, e''_q	transient, subtransient quadrature internal voltage.
e'_d, e''_d	transient, subtransient direct internal voltage;
L'_q, L''_q	transient, subtransient quadrature inductance;
L'_d, L''_d	transient, subtransient direct inductance;
L_l	leakage inductance;
T'_{do}	transient open-circuit, direct time constant;
T''_{do}	subtransient open-circuit, direct time constant;
T'_{qo}	transient open-circuit, quadrature time constant;
T''_{qo}	subtransient open-circuit, quadrature time constant.

Algebraic Equations [27]: Under the assumption that the voltage characteristics of loads are represented by a constant impedance model, the network calculation becomes a simple

linear calculation. First, the direct and quadrature internal voltages at node i on the rotator side, e_{gdi}, e_{gqi}, are given as

$$e_{gdi} = K_q \frac{L'_q - L''_q}{L'_q - L_l} e''_{di} + \frac{L''_q - L_l}{L'_q - L_l} e'_{di} \tag{12}$$

$$e_{gqi} = K_d \frac{L'_d - L''_d}{L'_d - L_l} e''_{qi} + \frac{L''_d - L_l}{L'_d - L_l} e'_{qi}. \tag{13}$$

These internal voltages can be transformed to the stator side, E_{GDi}, E_{GQi}, as follows:

$$\begin{bmatrix} E_{GDi} \\ E_{GQi} \end{bmatrix} = \begin{bmatrix} \sin\delta_i & \cos\delta_i \\ -\cos\delta_i & \sin\delta_i \end{bmatrix} \begin{bmatrix} e_{gdi} \\ e_{gqi} \end{bmatrix}. \tag{14}$$

Then, we can derive the network voltage and current by solving the following linear algebraic equations:

$$\begin{bmatrix} V_{Di} \\ V_{Qi} \end{bmatrix} = \begin{bmatrix} E_{GDi} \\ E_{GQi} \end{bmatrix} - \begin{bmatrix} Z'_{11i} & Z'_{12i} \\ Z'_{21i} & Z'_{22i} \end{bmatrix} \begin{bmatrix} I_{Di} \\ I_{Qi} \end{bmatrix} \tag{15}$$

$$\begin{bmatrix} I_{D1} \\ I_{Q1} \\ \vdots \\ I_{DN} \\ I_{QN} \end{bmatrix} = \begin{bmatrix} G_{11} & -B_{11} & \dots & G_{1N} & -B_{1N} \\ B_{11} & G_{11} & \dots & B_{1N} & G_{1N} \\ \vdots & \vdots & \ddots & \vdots & \vdots \\ G_{N1} & -B_{N1} & \dots & G_{NN} & -B_{NN} \\ B_{N1} & G_{N1} & \dots & B_{NN} & G_{NN} \end{bmatrix} \begin{bmatrix} V_{D1} \\ V_{Q1} \\ \vdots \\ V_{DN} \\ V_{QN} \end{bmatrix} \tag{16}$$

where

$Z'_{11i}, Z'_{12i}, Z'_{21i}, Z'_{22i}$	output impedance;
G_{ii}, B_{ii}	driving-point conductance, susceptance at node i;
G_{ij}, B_{ij}	transfer conductance, susceptance at branch i-j;
I_{Di}, I_{Qi}	direct, quadrature-injected current;
V_{Di}, V_{Qi}	direct, quadrature voltage.

APPENDIX B
BASIC EQUATIONS FOR WAVEFORM RELAXATION METHOD

In the waveform relaxation method, the original problem is divided into multiple subproblems in space, and each problem is assigned to different processor. On the border of the adjoining subproblems, the interface variables, which are called waveforms, are defined as shown in Fig. 13. The entire time domain is also divided into multiple time windows. DAE for each subproblem is solved independently from those of other subproblems for each time window, then the waveform information is exchanged between adjoining subproblems. If the update of the waveform converges, the calculation proceeds to the next time window.

The specific algorithm is as follows:

Step 0: The original system is divided into multiple subsystems based on the partitioning points. The number of subsystems is defined as N_s. The entire time domain $[0, T]$ is also divided into multiple time windows, $[T_{tw}, T_{tw+1}]$. Set $k = 1$.

Step 1: Estimate the initial waveform of each subsystem s, $w_s^k(t) : t \in [t_{tw}, t_{tw+1}]$, by using the linear calculation proposed in [1]–[3].

Step 2: Solve DAE for each subsystem s described by the following equation based on the Gauss-Jacobi relaxation method:

$$\begin{cases} y'^k_s &= f(y^k_s, z^k_s, w^{k-1}_{sa}, t),\ t \in [t_{tw}, t_{tw+1}] \\ 0 &= g(y^k_s, z^k_s, w^{k-1}_{sa}, t) \end{cases} \tag{17}$$

where

y_s^k	differential variables at iteration k, subsystem s;
z_s^k	algebraic variables at iteration k, subsystem s;
w_{sa}^{k-1}	waveform at subsystems adjoining subsystem s at iteration $k-1$.

Step 3: If the following convergence condition is satisfied, end the calculation:

$$e_{\max} = \max_{t_i \in [t_{tw}, t_{tw+1}]} \left(|w_s^k(t_i) - w_s^{k-1}(t_i)| \right) < e_{th} \tag{18}$$

where $e_{\max}, e_{th}$ is the maximum and allowable value of the correction, or set $k = k + 1$ and go to step 1 again.

See [4] for details on the waveform relaxation method.

REFERENCES

[1] F. Pruvost, P. Laurent-Gengoux, F. Magoulès, and B. Haut, "Accelerated waveform relaxation methods for power systems," in *Proc. 2011 Int. Conf. Electrical and Control Eng. (ICECE2011)*, 2011, vol. 4.

[2] F. Pruvost, T. Cadeau, P. Laurent-Gengoux, F. Magoulès, F.-X. Bouchez, and B. Haut, "Numerical accelerations for power systems transient stability simulations," in *Proc. 17th Power Syst. Computat. Conf. (PSCC2011)*, 2011.

[3] F. Pruvost, P. Laurent-Gengoux, F. Magoulès, and F.-X. Bouchez, "Speed-up the computing efficiency of waveform relaxation method for power system transient stability," in *Proc. 1st Int. Workshop High Performance Comput., Network. and Analytics for the Power Grid*, 2011, pp. 11–18.

[4] E. Lelarasmee, "The waveform relaxation method for time-domain analysis of large scale integrated circuits," *IEEE Trans. Comput.-Aided Design Integr. Circuits Syst.*, vol. 1, no. 3, pp. 131–145, 1982.

[5] K. Burrage, Z. Jackiewicz, S. P. Nørsett, and R. A. Renaut, "Preconditioning waveform relaxation iterations for differential systems," *BIT Numer. Math.*, vol. 36, no. 1, pp. 54–76, 1996.

[6] L. Halpern, "Absorbing boundary conditions and optimized Schwarz waveform relaxation," *BIT Numer. Math.*, vol. 43, no. 1, pp. 1–18, 2003.

[7] M. J. Gander and A. E. Ruehli, "Optimized waveform relaxation methods for RC type circuits," *IEEE Trans. Circuits Syst. I*, vol. 51, no. 4, pp. 755–768, 2004.

[8] D. S. Daoud and M. J. Gander, "Overlapping Schwarz waveform relaxation for advection reaction diffusion problems," *Bol. Soc. Esp. Mat. Apl.*, vol. 46, pp. 75–90, 2009.

[9] F. Magoulès, P. Laurent-Gengoux, and F. Pruvost, "Preconditioners for Schwarz relaxation methods applied to differential algebraic equations," *Int. J. Comput. Math.*, vol. 91, no. 8, pp. 1775–1789, 2014.

[10] M. J. Gander and S. Vandewalle, "Analysis of the parallel time-parallel time-integration method," *SIAM J. Sci. Comput.*, vol. 29, no. 2, pp. 556–578, 2007.

[11] T. Cadeau and F. Magoulès, "Coupling parallel and waveform relaxation methods for power systems," in *Proc. 2011 Int. Conf. Electrical and Control Eng. (ICECE2011)*, 2011, vol. 4.

[12] T. Cadeau and F. Magoulès, "Coupling the parallel algorithm with the waveform relaxation method for the solution of differential algebraic equations," in *Proc. 10th Int. Symp. Distributed Comput. and Applicat. to Business, Eng. and Sci. (DCABES)*, 2011.

[13] G. Karypis and V. Kumar, "METIS a software package for partitioning unstructured graphs," *Partitioning Meshes, and Computer Fill-Reducing Orderings of Sparse Matrices, Version 4.0*, 1998.

[14] J. Shu, W. Xue, and W. Zheng, "A parallel transient stability simulation for power systems," *IEEE Trans. Power Syst.*, vol. 20, no. 4, pp. 1709–1717, Nov. 2005.

[15] M. L. Crow and M. Ilic, "The parallel implementation of the waveform relaxation method for transient stability simulations," *IEEE Trans. Power Syst.*, vol. 5, no. 3, pp. 922–932, Aug. 1990.
[16] L. Hou and A. Bose, "Implementation of the waveform relaxation algorithm on a shared memory computer for the transient stability problem," *IEEE Trans. Power Syst.*, vol. 12, no. 3, pp. 1053–1060, Aug. 1997.
[17] N. Zhu and A. Bose, "A dynamic partitioning scheme for parallel transient stability analysis," *IEEE Trans. Power Syst.*, vol. 7, no. 2, pp. 940–946, May 1992.
[18] T. Stephen, Y. Lee, and F. C. Schweppe, "Distance measures and coherency recognition for transient stability equivalents," *IEEE Trans. Power App. Syst.*, vol. PAS-92, no. 5, pp. 1550–1557, 1973.
[19] M. A. M. Ariff and B. C. Pal, "Coherency identification in interconnected power system: An independent component analysis approach," *IEEE Trans. Power Syst.*, vol. 28, no. 2, pp. 1747–1755, May 2013.
[20] F. B. Alhasawi and V. Milanović, "Ranking the importance of synchronous generators for renewable energy integration," *IEEE Trans. Power Syst.*, vol. 27, no. 1, pp. 416–423, Feb. 2012.
[21] H. Mehrjerdi, S. Lefebvre, M. Saad, and D. Asber, "A decentralized control of partitioned networks for voltage regulation and prevention against disturbance propagation," *IEEE Trans. Power Syst.*, vol. 28, no. 2, pp. 1461–1469, May 2013.
[22] K. Sun, K. Hur, and P. Zhang, "A new unified scheme for controlled power system separation using synchronized phasor measurements," *IEEE Trans. Power Syst.*, vol. 26, no. 3, pp. 1544–1554, Aug. 2011.
[23] N. Uchida, K. Kawata, and M. Egawa, "Development of test case models for Japanese power systems," in *Proc. 2000 IEEE PES Summer Meeting*, 2000.
[24] K. Takahashi *et al.*, Integrated Analysis Software for Bulk Power System Stability, 1991, CRIEPI Rep. ET90002.
[25] The Institute of Electrical Engineers of Japan (IEEJ), Japanese Power System Models [Online]. Available: http://www2.iee.or.jp/ver2/pes/23-st_model/english/index.html
[26] N. Kakimoto and K. Tomiyama, "Verification of autoparametric resonance in longitudinal power system," (in Japanese) *IEEJ Trans. Power Energy*, vol. 115, no. 3, pp. 219–226, 1995.
[27] P. Kundur, *Power System Stability and Control*. New York, NY, USA: McGraw-Hill Professional, 1994.

Takao Tsuji (M'13) received the Dr.Eng. degree from Yokohama National University, Japan, in 2006.

In April of the same year, he was appointed as a Research Associate in the Graduate School of Information Science and Electrical Engineering of Kyushu University. Since April of 2007, he has been with the Faculty of Engineering at Yokohama National University, Japan, and is currently an Associate Professor. His research interests include the planning, operation, and control of electric power systems.

Prof. Tsuji is a member of IEEJ.

Frédéric Magoulès (M'13) received the B.Sc. degree in engineering sciences, the M.Sc. degree in applied mathematics, the M.Sc. degree in numerical analysis, and the Ph.D. degree in applied mathematics from Université Pierre & Marie Curie, France, in 1993, 1994, 1995, and 2000, respectively.

He is currently a Professor in the Department of Mathematics and in the Department of Computer Science at Ecole Centrale Paris, France. His research interests include numerical analysis and simulation of power systems.

Prof. Magoulès is a Fellow of IMA and a member of SIAM.

Kenko Uchida (M'89) received the B.S., M.S., and Dr.Eng. degrees in electrical engineering from Waseda University, Japan, in 1971, 1973, and 1976, respectively.

He is currently a Professor in the Department of Electrical Engineering and Bioscience, Waseda University. His research interests are in robust/optimization control and control problems in energy systems and biology.

Prof. Uchida is a member of SICE and IEEJ.

Tsutomu Oyama (S'78–M'84) received the B.S., M.S., and Dr.Eng. degrees in electrical engineering from the University of Tokyo, Tokyo, Japan, in 1978, 1980, and 1983, respectively.

Since 1983, he has been with Yokohama National University, Japan, where is currently a Professor. His research interests include the analysis, operation, and planning of power systems.

Prof. Oyama is a member of CIGRE, Japan Society of Energy and Resources, and IEE of Japan.